INVESTIGATIONS OF A RECONFIGURABLE PRESSING SETUP FOR MANUFACTURING BLADES OF LARGE FRANCIS TURBINES RUNNERS FROM VERY THICK PLATES

Zhengkun Feng [a✧], Henri Champliaud [b], Louis Mathieu [c]

[a, b] Mechanical Engineering Department, Ecole de technologie superieure, 1100 Notre-Dame West, Montreal, Quebec, H3C 1K3, Canada
[c] GE Hydro, 1350 St-Roch Road, Sorel-Tracy, Quebec, J3P 5P9, Canada

[b]henri.champliaud@etsmtl.ca, [c]louis.mathieu@power.alstom.com

ABSTRACT

The design of Francis turbines of hydropower plants is not standard, but different from one site to another due to hydraulic conditions. As a result, the hydraulic profile and the size of the blades of each Francis turbine are different. Therefore, the blades, one of the key components of Francis turbine runners, are produced in small batches and the setup of the dedicated punch and die increases significantly the unit production cost. In this paper, a flexible pressing process with reconfigurable punch and die for very thick plates is investigated. Firstly, a model for pressing very thick plates by conventional pressing process with matched punch and die is built. The simulation results agree well with the data obtained during a recent rehabilitation of a hydropower plant in Quebec. The results obtained from the model of the flexible pressing process are compared with the conventional pressing process.

Keywords: Pressing process; Multi-point forming; Finite element analysis; Very thick plate; Reconfigurable punch

1. INTRODUCTION

The pressing process has many advantages over the casting process and is widely used in automotive, shipbuilding, energy production and civil engineering. In casting process, gas entrapment may occur during mold filling (Wang et al. 2013) and an excessive amount of gases may result in gas porosity defect (Perzyk and Kochański, 2003). Consequently, the pressing process becomes an alternative of the casting process. For hydroelectricity, the blades of a Francis turbine runner (Fig. 1) can be produced by forming. This process reduces the manufacture time and cost. In addition, operators require less experience for the final machining (Casacci et al., 1977; Casacci and Caillot, 1983). Then a conventional pressing process with matched punch and die is actually used for manufacturing blades. Firstly, the pressing process provides a raw blade with constant thickness from a flat plate (Fig.2a). Then, after an operator machines this raw blade to a blade with the required size and hydro profile it is inspected (Fig. 2b) for geometry compliance.

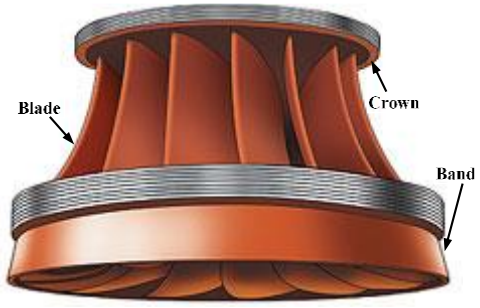

Fig. 1 Francis turbine runner composed of blade and other elements (Source from Hydro-Quebec)

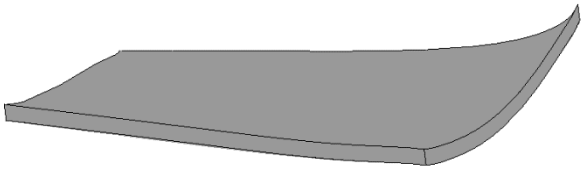

(a) A raw blade;

(b) Inspection of a raw blade after machining

Fig. 2 Manufacture of a raw blade to a blade with hydro profiles from a raw blade.

However, the design of Francis turbines is not standard and may be very different from one site to another due to hydraulic conditions. As a result, the hydraulic profile, the size and the thickness of the blades of the runner are different from one Francis turbine to another. Therefore, the blades, one of the key components of a Francis turbine runner, are produced in

small batches. The conventional pressing process with matched punch and die affects significantly the unit production cost. In addition, the trial and error technique that is practiced for thin plate and mass production becomes very costly for pressing of very thick plates and small production batches due to the intensive time and energy consuming. The flexible pressing process or multi-point pressing process with reconfigurable punch and die can save design and manufacturing time and attracts increasingly considerations for the manufacture of components with high thickness.

In the early 1980's, Hardt et al. (1981) investigated the multi-point forming process through various experiments. Until the late 1990's and the early 2000's, the focus was still on mechanical design and manufacturing of reconfigurable dies. Li et al. (1999) reported various multi-point forming processes. Closely packed pins to withstand the forming load were applied by Walczyk and Hardt (1998, 1999) and sectional multi-point forming was applied by Li et al. (2002). Papazian (2002) reported the very fast full reconfiguration of the die. With the rapid evolution of computer and computing technology, robust metal forming machines become possible. High efficient computational method and computing technique make the design of this kind of machine easier. Numerical simulations with explicit scheme (Li et al., 2002) and with implicit scheme (Chen et al., 2005) for sectional multi-point forming, with implicit scheme for multi-point forming (Cai and Li, 2005) were performed. Recently, the multi-point forming for cylindrical and spherical sections (Quan et al., 2011), double curved saddle section (Heo et al., 2010a, 2010b) were reported. Tests and numerical simulations on small scale and simple workpieces were carried out by Davoodi et al. (2014).

This study aims to investigate the pressing process for manufacturing the raw blades from very thick plates. The thickness of the plates is constant and so is the thickness of the raw blades obtained from the pressing process. The hydraulic profile with varied thickness is obtained by machining the pressed blank with a 5-axis CNC milling machine and by a final grinding stage (Sabourin et al., 2010) as shown in Fig.3.

Fig. 3 Robotic grinding of a Francis turbine runner blade (Sabourin et al., 2010).

In this paper, the modeling of the conventional pressing process with matched punch and die is given. The simulation results from this model are compared with the data obtained from the recent rehabilitation of a hydropower plant in Quebec, Canada. The proposed flexible pressing process with reconfigurable punch and die is investigated and the simulation results are compared with those obtained from the conventional pressing process with matched punch and die.

2. MODELING AND SIMULATION OF PRESSING PROCESS WITH MATCHED PUNCH AND DIE FOR VERY THICK PLATES

The numerical model of the pressing process with matched punch and die for thick plates is shown in Fig. 4. The model was composed of a flat blank, a matched punch, a matched die and pressing guides that are used to prevent the blank from moving out of the pressing machine. The material of the blank was the stainless steel ASTM A743 grade CA6NM. The elastic perfectly plastic material model at temperature of 800 °C was used for the blank. At this temperature the Young's modulus, the yield stress, the Poisson's ratio and the density were 92 GPa, 134 MPa, 0.3, 7850 kg/m^3, respectively. The punch, the die and the pressing guides were assumed as rigid bodies. The top and the bottom surfaces of the punch and die were identical to those of the desired raw blade. Therefore, the deformed shape of the raw blade was going to have the extrados on the top and intrados on the bottom. The blank, the punch and the die had thickness of 102 mm and were meshed with linear 8-node solid elements. Both top and bottom surfaces of the blank were more than 4 m^2. The thickness of the pressing guides was assumed to be very small and was meshed with linear 4-node shell elements with five integration points through the thickness. The static and dynamic friction coefficients between the blank and the punch, the die and the pressing guides were 0.6, respectively. The contact type between the blank and the punch and between the blank and the die was automatic surface to surface with the surfaces of the rigid bodies as contact surfaces and the surfaces of the blank as target surfaces. The contact type between the blank and the pressing guides was automatic node to surface contact with the nodes of the pressing guides as contact nodes and the surfaces of the blank as contact surfaces. As the thickness of the pressing guides was very small their nodes were very close to the blank surfaces. For the sake of CPU time, the simulation time was selected as 1 second. Figure 5 shows the shape of the blade obtained with the FE model. Figure 6 shows the strain distributions in six layers of the deformed blade that was divided by the six elements in the thickness. The layer order was from the bottom for the first layer to the top for the sixth layer. Figure 7 shows the time history of the applied force, i.e., the pressing force. Evidently, this force increased rapidly during the final stage of the pressing process. The red point indicated the maximum value of the pressing force of the pressing machine (see the following section).

ISBN 978-88-97999-85-0; Affenzeller, Bruzzone, Jiménez, Longo and Piera Eds.

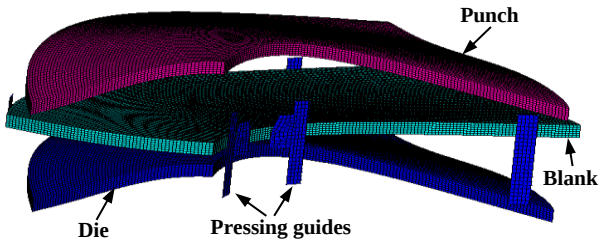

Fig. 4 Model of the pressing process with matched punch and die.

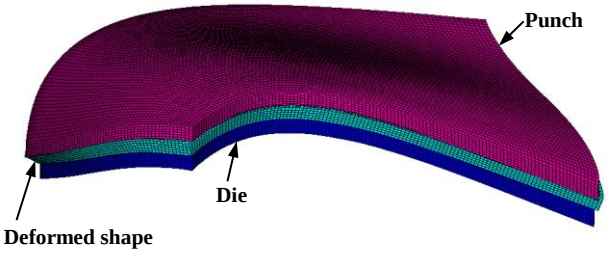

Fig. 5 Raw blade deformed by the matched punch and die.

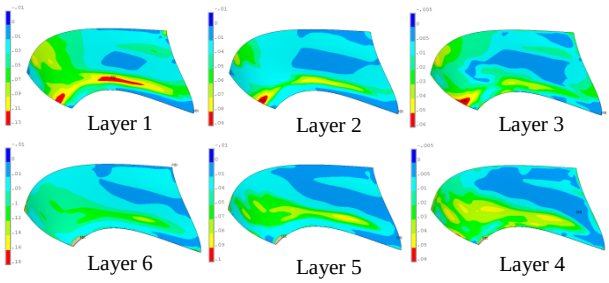

Fig. 6 Strain distributions at six layers of the deformed shape.

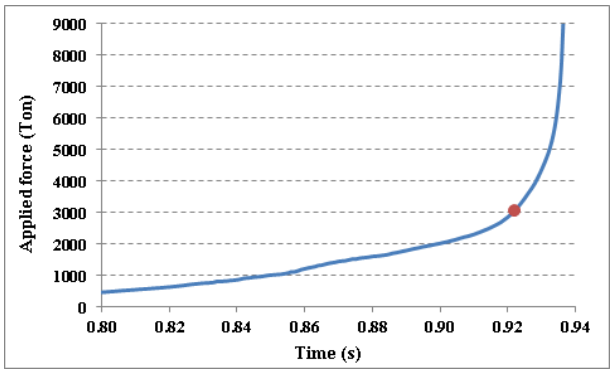

Fig. 7 Pressing force during hot blade pressing.

3. COMPARISON BETWEEN NUMERICAL RESULTS AND MANUFACTURING DATA

The application of the pressing process with matched punch and die was performed to manufacture the blades of Francis turbine runners used in the rehabilitation of Hydro-Quebec's historic Beauharnois power station. The maximum pressing force of the pressing machine was 3000 Tons (Fig. 7) and this value was reached at the final instant of the pressing process. The final displacements of two raw blades to the blanks were measured and were saved for the comparison with the numerical results obtained from the simulations as described in the previous sections. The locations of the measurement points on the extrados and intrados of the raw blades are illustrated in Fig. 8. There were 81 measurement points that are regularly spaced in 9 rows and 9 columns on both extrados and intrados of the raw blades. Although there were two points without available values on both extrados and intrados of the raw blades, the rest 79 measurement points allowed the performance of the comparisons.

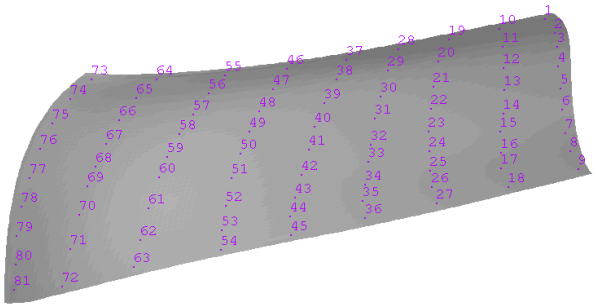

(a) On the extrados;

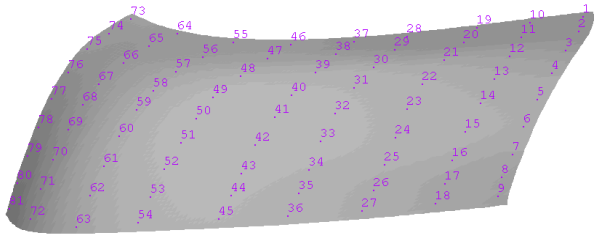

(b) On the intrados;

Fig. 8 Measurement point locations on the raw blade obtained by the pressing machine

Figure 9 and Figure 10 show the differences between the simulation results and the manufacturer's data at the location of each measurement point on both extrados and intrados of the two raw blades. In these figures, a negative value was an insufficient displacement value of the simulation result at this point. For example, in Fig. 9, from point 10 to point 19 and from point 20 to point 27, there was not enough displacements, and from point 46 to point 54 and from point 55 to point 63, there was too much displacements. Tables 1-4 show the differences between the simulation results and the inspection data at each measurement point of the two raw blades on both extrados and intrados. The maximum values located at points 37, 46 and the minimum values located at points 9, 25, 26. The locations of these points were on or near the edges of the raw blades where the thickness was small for the required hydro profile of the blades. Therefore, these differences could not prevent from obtaining the blades with desired hydro profiles by machining the raw blades. Table 5 gives the maximum differences of these values on these two raw blades. Both the maximum and minimum values were less than 1 cm for a thickness of more than 10 cm. Therefore, the simulation results compared well with the manufacture data.

ISBN 978-88-97999-85-0; Affenzeller, Bruzzone, Jiménez, Longo and Piera Eds.

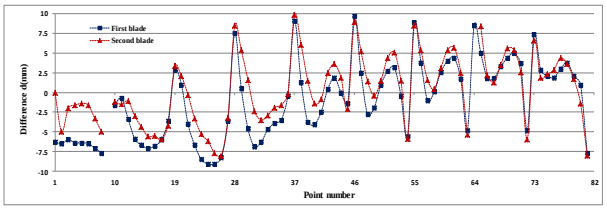

Fig. 9 Extrados difference between the simulation results and the manufacturer's data for the two blades.

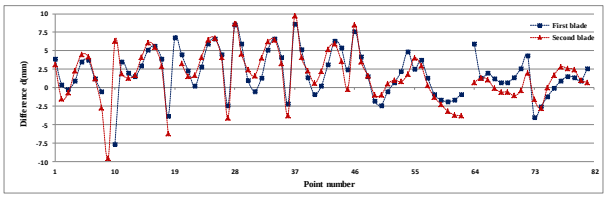

Fig. 10 Intrados difference between the simulation results and the manufacturer's data for the two blades.

Table 1: Position differences between simulations and test results for the extrados of the first raw blade

Point No	*1*	*2*	*3*	*4*	*5*	*6*	*7*	*8*	*9*
d(mm)	**-6.3**	**-6.5**	**-6**	**-6.4**	**-6.4**	**-6.5**	**-7.1**	**-7.7**	/
Point No	*10*	*11*	*12*	*13*	*14*	*15*	*16*	*17*	*18*
d(mm)	**-1.6**	**-0.7**	**-3.4**	**-5.9**	**-6.7**	**-7.1**	**-6.8**	**-6**	**-3.6**
Point No	*19*	*20*	*21*	*22*	*23*	*24*	*25*	*26*	*27*
d(mm)	**2.9**	**1**	**-4**	**-6.7**	**-8.5**	**-9.1**	**-9.1**	**-8.3**	**-3.6**
Point No	*28*	*29*	*30*	*31*	*32*	*33*	*34*	*35*	*36*
d(mm)	**7.5**	**0.5**	**-4.6**	**-6.9**	**-6.3**	**-4.7**	**-3.9**	**-3.5**	**-0.4**
Point No	*37*	*38*	*39*	*40*	*41*	*42*	*43*	*44*	*45*
d(mm)	**9.1**	**1.3**	**-3.8**	**-4.1**	**-2.5**	**0.4**	**1.9**	**0**	**-1.4**
Point No	*46*	*47*	*48*	*49*	*50*	*51*	*52*	*53*	*54*
d(mm)	**9.7**	**2.5**	**-2.8**	**-1.9**	**1**	**2.7**	**3.2**	**-0.4**	**-5.6**
Point No	*55*	*56*	*57*	*58*	*59*	*60*	*61*	*62*	*63*
d(mm)	**8.9**	**3.8**	**-1**	**0.1**	**2.6**	**4**	**4.4**	**1.7**	**-4.8**
Point No	*64*	*65*	*66*	*67*	*68*	*69*	*70*	*71*	*72*
d(mm)	**8.5**	**5**	**1.8**	**1.8**	**3.3**	**4.4**	**5**	**3.7**	**-4.8**
Point No	*73*	*74*	*75*	*76*	*77*	*78*	*79*	*80*	*81*
d(mm)	**7.4**	**2.9**	**2.1**	**1.9**	**3**	**3.8**	**2.1**	**1**	**-7.7**

Table 2: Position differences between simulations and test results for the intrados of the first raw blade

Point Nº	*1*	*2*	*3*	*4*	*5*	*6*	*7*	*8*	*9*
d(mm)	**3.9**	**0.4**	**-0.2**	**0.9**	**3.5**	**3.7**	**1.2**	**-0.5**	**-7.7**
Point Nº	*10*	*11*	*12*	*13*	*14*	*15*	*16*	*17*	*18*
d(mm)	/	**3.5**	**2.0**	**1.5**	**3.0**	**5.1**	**5.6**	**3.9**	**-3.9**
Point Nº	*19*	*20*	*21*	*22*	*23*	*24*	*25*	*26*	*27*
d(mm)	**6.8**	**4.5**	**2.3**	**0.2**	**2.8**	**5.9**	**6.6**	**4.5**	**-2.4**
Point Nº	*28*	*29*	*30*	*31*	*32*	*33*	*34*	*35*	*36*
d(mm)	**8.5**	**5.9**	**1.0**	**-0.5**	**1.3**	**5.1**	**6.6**	**4.1**	**-2.2**
Point Nº	*37*	*38*	*39*	*40*	*41*	*42*	*43*	*44*	*45*
d(mm)	**8.6**	**5.2**	**1.4**	**-0.9**	**0.2**	**3.1**	**6.3**	**5.4**	**2.4**
Point Nº	*46*	*47*	*48*	*49*	*50*	*51*	*52*	*53*	*54*
d(mm)	**7.6**	**4.2**	**1.5**	**-1.8**	**-2.4**	**-0.5**	**0.7**	**2.2**	**4.9**
Point Nº	*55*	*56*	*57*	*58*	*59*	*60*	*61*	*62*	*63*
d(mm)	**2.5**	**3.7**	**1.3**	**-0.9**	**-1.7**	**-1.9**	**-1.7**	**-0.9**	**5.9**
Point Nº	*64*	*65*	*66*	*67*	*68*	*69*	*70*	*71*	*72*
d(mm)	/	**1.3**	**2**	**1.2**	**0.7**	**0.7**	**1.4**	**2.6**	**4.3**
Point Nº	*73*	*74*	*75*	*76*	*77*	*78*	*79*	*80*	*81*
d(mm)	**-4.0**	**-2.6**	**-1.2**	**-0.1**	**0.9**	**1.5**	**1.4**	**0.9**	**2.6**

Table 3: Position differences between simulation and test results for the extrados of the second raw blade

Point Nº	*1*	*2*	*3*	*4*	*5*	*6*	*7*	*8*	*9*
d(mm)	**0.0**	**-5.0**	**-2.0**	**-1.6**	**-1.4**	**-1.6**	**-3.3**	**-5.0**	/
Point Nº	*10*	*11*	*12*	*13*	*14*	*15*	*16*	*17*	*18*
d(mm)	**-1.2**	**-1.5**	**-1.1**	**-3.0**	**-4.4**	**-5.6**	**-5.5**	**-6.0**	**-4.2**
Point Nº	*19*	*20*	*21*	*22*	*23*	*24*	*25*	*26*	*27*
d(mm)	**3.4**	**2.1**	**-0.3**	**-3.3**	**-5.3**	**-6.2**	**-7.7**	**-8.1**	**-3.2**
Point Nº	*28*	*29*	*30*	*31*	*32*	*33*	*34*	*35*	*36*
d(mm)	**8.5**	**5.4**	**1.6**	**-2.4**	**-3.5**	**-2.9**	**-1.9**	**-1.6**	**-0.2**
Point Nº	*37*	*38*	*39*	*40*	*41*	*42*	*43*	*44*	*45*
d(mm)	**9.9**	**6.1**	**1.5**	**-1.4**	**-0.9**	**2.5**	**3.6**	**1.9**	**-2.1**
Point Nº	*46*	*47*	*48*	*49*	*50*	*51*	*52*	*53*	*54*
d(mm)	**9.0**	**5.2**	**1.4**	**-0.4**	**1.5**	**4.4**	**5.1**	**1.5**	**-5.9**
Point Nº	*55*	*56*	*57*	*58*	*59*	*60*	*61*	*62*	*63*
d(mm)	**8.5**	**5.4**	**1.6**	**0.4**	**3.1**	**5.4**	**5.7**	**2.5**	**-5.4**
Point Nº	*64*	*65*	*66*	*67*	*68*	*69*	*70*	*71*	*72*
d(mm)	**8.4**	/	**2.2**	**1.3**	**3.5**	**5.6**	**5.4**	**2.6**	**-6.0**
Point Nº	73	74	75	76	77	78	79	80	81
d(mm)	**6.6**	**1.9**	**2.3**	**2.9**	**4.4**	**3.6**	**1.7**	**-1.4**	**-8.0**

Table 4: Position differences between simulations and test results for the intrados of the second raw blade

Point Nº	*1*	*2*	*3*	*4*	*5*	*6*	*7*	*8*	*9*
d(mm)	**3.1**	**-1.5**	**-0.7**	**2.3**	**4.5**	**4.2**	**1.2**	**-2.7**	**-9.6**
Point Nº	*10*	*11*	*12*	*13*	*14*	*15*	*16*	*17*	*18*
d(mm)	**6.3**	**1.9**	**1.3**	**1.7**	**4.1**	**6.1**	**5.5**	**2.9**	**-6.2**
Point Nº	*19*	*20*	*21*	*22*	*23*	*24*	*25*	*26*	*27*
d(mm)	/	**3.3**	**1.5**	**1.7**	**4.1**	**6.5**	**6.7**	**4.1**	**-4.1**
Point Nº	*28*	*29*	*30*	*31*	*32*	*33*	*34*	*35*	*36*
d(mm)	**8.7**	**4.6**	**2.4**	**1.6**	**4.0**	**6.2**	**6.5**	**3.3**	**-3.8**
Point Nº	*37*	*38*	*39*	*40*	*41*	*42*	*43*	*44*	*45*
d(mm)	**9.7**	**4.1**	**2.3**	**0.6**	**2.2**	**5.2**	**5.9**	**3.6**	**-0.2**
Point Nº	*46*	*47*	*48*	*49*	*50*	*51*	*52*	*53*	*54*
d(mm)	**8.5**	**3.5**	**1.6**	**-1.0**	**-1.0**	**0.5**	**1.0**	**0.8**	**1.8**
Point Nº	*55*	*56*	*57*	*58*	*59*	*60*	*61*	*62*	*63*
d(mm)	**4.0**	**3.0**	**0.3**	**-1.3**	**-2.3**	**-3.2**	**-3.7**	**-3.8**	**0.7**
Point Nº	*64*	*65*	*66*	*67*	*68*	*69*	*70*	*71*	*72*
d(mm)	/	**1.3**	**1.1**	**-0.1**	**-0.6**	**-0.6**	**-1.1**	**-0.4**	**2.0**
Point Nº	*73*	*74*	*75*	*76*	*77*	*78*	*79*	*80*	*81*
d(mm)	**-1.6**	**-2.8**	**0.0**	**1.7**	**2.8**	**2.6**	**2.4**	**1.0**	**0.7**

Table 5: Maximum position differences between simulations and test results

	First blade		**Second blade**	
	min d (mm)	**max d (mm)**	**min d (mm)**	**max d (mm)**
Extrados	**-9.1**	**9.7**	**-8.1**	**9.9**
Intrados	**-7.7**	**8.6**	**-9.6**	**9.7**

ISBN 978-88-97999-85-0; Affenzeller, Bruzzone, Jiménez, Longo and Piera Eds.

4. GEOMETRY SET UP OF THE PRESSING PROCESS WITH RECONFIGURABLE PUNCH AND DIE

A multi-point pressing process consists mainly of a reconfigurable punch, a reconfigurable die and a workpiece, i.e., a blank. A simple example in two dimensions is shown in Fig. 11. The punch and die are composed of arrays of various pins with adjustable positions. During the pressing process the die is motionless and the punch applied a downward force on the workpiece through the contact point between each pin and the workpiece to deform it. The shape of a pin is a cylinder with a semi-sphere at one end that is used to deform the workpiece at the contact point. In comparison with the workpiece, the deformation of the tool is very small and can be neglected. Therefore, the cylindrical parts of the pins are not considered in the following text for simplicity and only the pin ends are reprensented in the model.

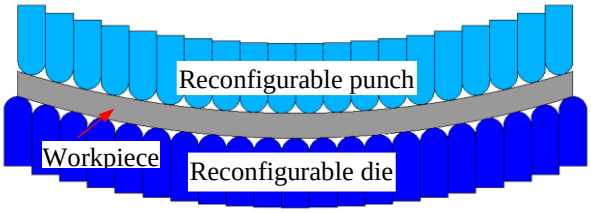

Fig. 11 Schematic diagram of a two-dimensional multi-point press process.

Figure 12 illustrates the geometry of the proposed multi-point pressing process with a reconfigurable punch and a reconfigurable die for producing raw blades. The upper matrix is the punch and the lower matrix is the die. The vertical direction is defined as the z direction in the geometry set up. Initially, the blank lies horizontally on the motionless die, i.e., in the xy plane. The top and bottom surfaces of the deformed shape correspond to the extrados and the intrados of the raw blade, respectively. The pressing zone for the punch and die are determined by the extrados and intrados of the raw blade. The pressing machine has an upper array of pins with the downward ends used for the punch and a lower array of pins with the upward ends used for the die. The positions and the number of pins used for the punch and die are determined by the shape of the desired shape, i.e., the raw shape of the blade. The positions of the pins of the reconfigurable punch are determined by the extrados of the raw blade and those of the reconfigurable die are determined by the intrados of the raw blade. The determination of the positions and the number of pins of the reconfigurable punch is given in the following subsections. The determination of the positions and the number of pins for the reconfigurable die is very similar and will not be repeated here.

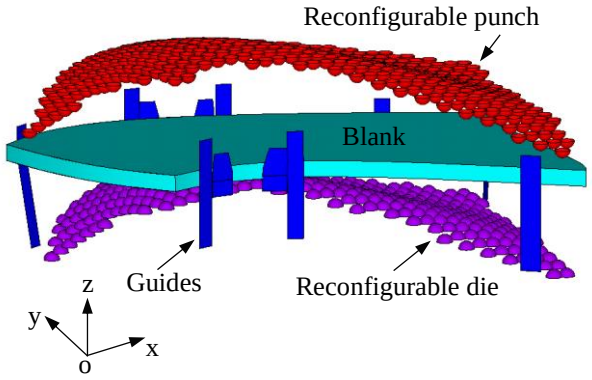

Fig. 12 Geometry of the multi-point pressing process.

4. 1 Determination of the number of pins

Figure 13 shows the upper array of 33x33 pins. Only the pins in the punch pressing zone are selected for building the reconfigurable punch. The relative positions of the pins to the extrados of the raw blade are illustrated in Fig. 14. However, the blank to be deformed is larger than the punch pressing zone Fig. 15. For ensuring the quality of the deformed shape, the pins of the punch pressing zone has to cover the extrados of the raw blank.

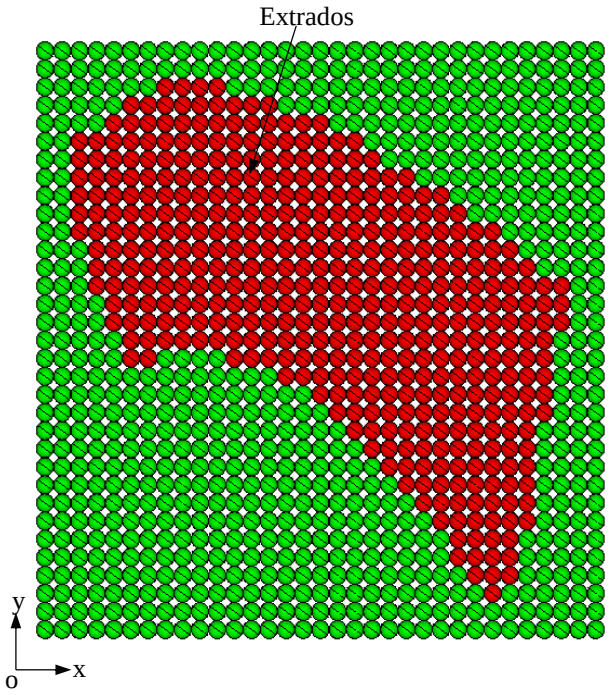

Fig. 13 Upper array of the pins of the pressing process

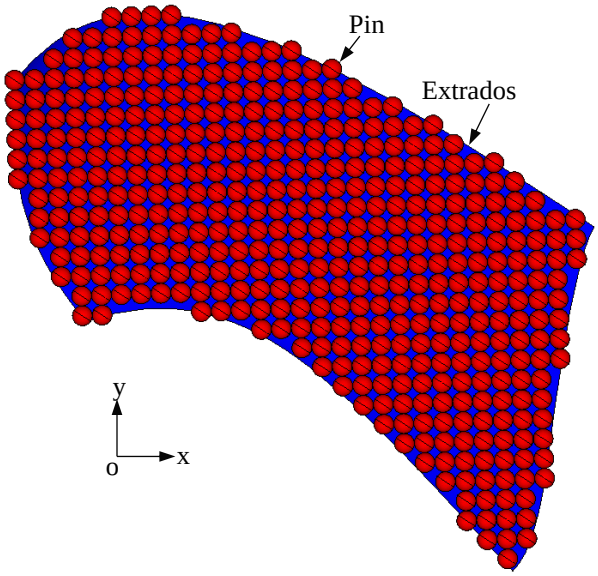

Fig. 14 Reconfigurable punch of the multi-point pressing process with the extrados of the desired raw blade.

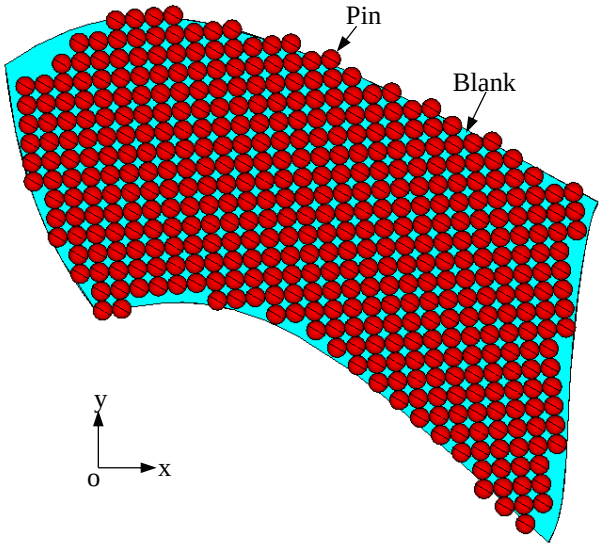

Fig. 15 Reconfigurable punch of the multi-point pressing process with the extrados of the blank to be deformed.

4.2 Determination of contact positions between the pins and the extrados of the raw blade

The positions of the pins of the punch are determined in the previous subsection. The x and y coordinates of the center of each pin are shown in Fig. 16 that is derived from Fig. 15. The coordinate in z direction (vertical direction) of each pin of the punch is determined in the following subsection.

Firstly, the extrados of the raw blade is divided by various triangles and these triangles are projected onto the xy plane as shown in Fig. 17. The center of the semi-sphere end of each pin locates in one of these triangles. Therefore, the x and y coordinates of these centers can be obtained from the positions of the centers of the semi-sphere ends of the pins in xy plane that are determined in the previous subsection.

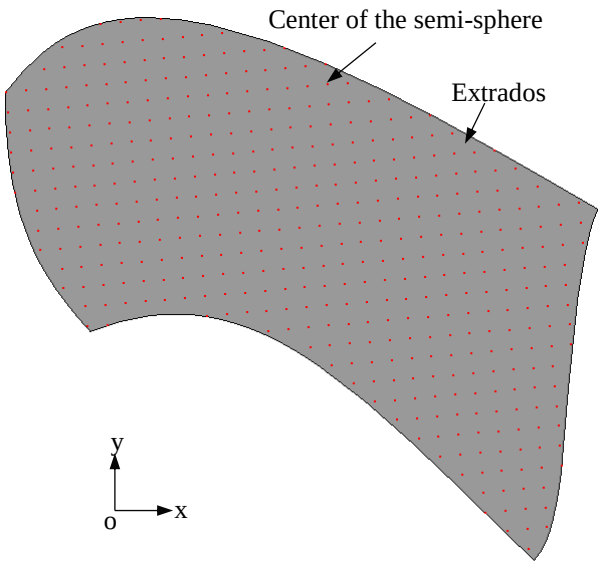

Fig. 16 Relative positions of the centers of the semi-sphere ends of the pins to the extrados of the raw blade.

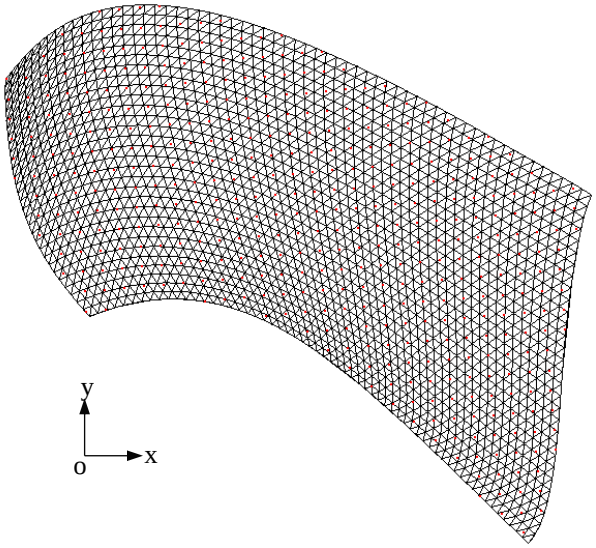

Fig. 17 Relative positions of the centers of the semi-sphere ends (red points) of the pins in the triangles that divided the extrados of the raw blade

For determining the z coordinate of the contact point of each pin, the following procedure can be performed. Firstly, select a center of the semi-sphere of a pin, following by selecting the triangles that the semi-sphere can cover with a margin to ensure the selection of all the triangles that among them one can be in contact with the semi-sphere as shown in Fig. 18 (from the top view, i.e., the view in the reverse z direction). Then, for each selected triangle, find the point in the plane of the triangle and verify if it locates in the triangle as shown in Fig. 19. In this figure the lines connecting points P_1, P_2 and P_3 represent the triangle. The line connecting P_4 and P_5 represents the axis of the pin, i.e., the pressing direction. Points P_6 and P_7 are the projected points of points P_4 and P_5 in the plane of the triangle, respectively. Note that points P_4, P_5, P_6 and P_7 are in the same plane. Finally,

ISBN 978-88-97999-85-0; Affenzeller, Bruzzone, Jiménez, Longo and Piera Eds.

point P_8 is on the straight line between points P_6 and P_7 that has a distance of the radius of the pin to the axis of the pin can be found. If ξ, η and ζ calculated from eqs. (1) to (3) are positives this point locates in the triangle. This triangle can have a contact point with the pin. The coordinates are those in the local coordinate system with the xy plane defined by the triangle.

$$\xi = \frac{(x_8 - x_1)(y_3 - y_1) - (x_3 - x_1)(y_8 - y_1)}{(x_2 - x_1)(y_3 - y_1) - (x_3 - x_1)(y_2 - y_1)} \quad (1)$$

$$\eta = \frac{(x_8 - x_1)(y_2 - y_1) - (x_2 - x_1)(y_8 - y_1)}{(x_3 - x_1)(y_2 - y_1) - (x_2 - x_1)(y_3 - y_1)} \quad (2)$$

$$\zeta = 1 - \xi - \eta \quad (3)$$

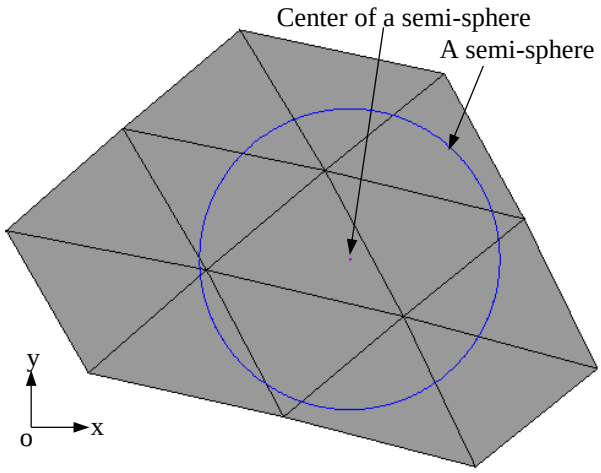

Fig. 18 Relative position of the centers of the semi-sphere end of a pin in a corresponding triangle.

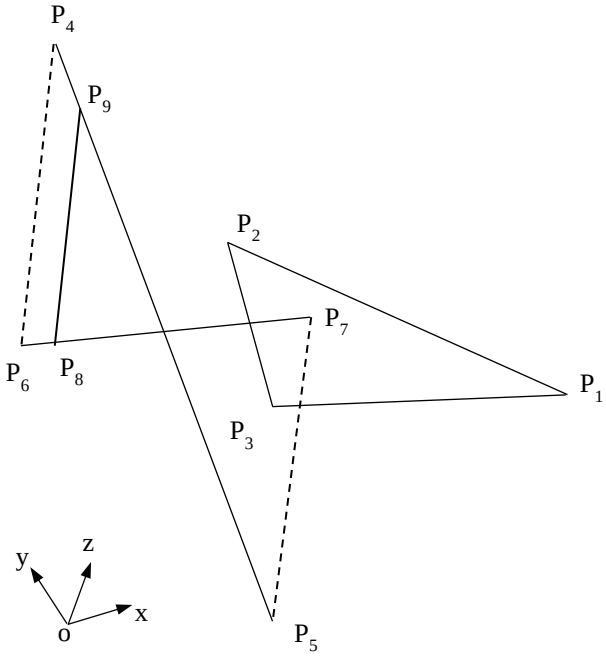

Fig. 19 Diagram for determining the distance of a triangle to the pin axis.

However, there may be more than one triangle that can have a contact point with the triangle. The one that has the biggest z coordinate in the global coordinate system (i.e., the pressing direction) is the real one. This triangle contacts with the pin when the punch moves downwards and this contact prevents the pin from contacting with the other triangles. The flow chart of the procedure to find the contact points between the extrados and the pins of the punch is illustrated in Fig. 20.

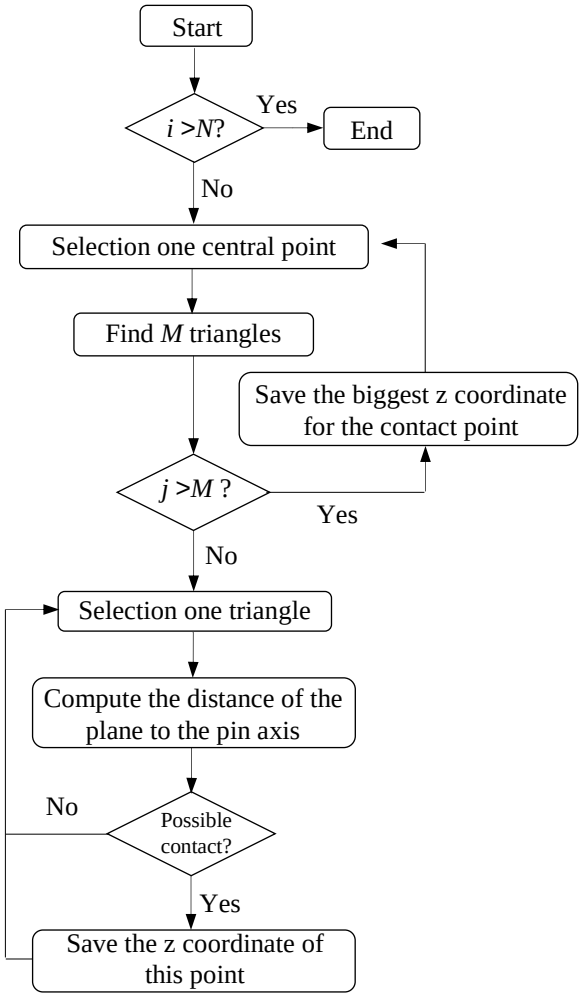

Fig. 20 Flow chart of finding the contact points between the extrados and the pins of the punch

In Fig. 20, the total number of pins is supposed to be N. The procedure starts with the first loop on the number of the pins. The center of the semi-sphere of the end of this pin is selected. Then the M triangles that have possibly contact points with the extrados are selected. The second loop on these selected triangles starts. Each triangle is checked to see if it is possibly in contact with the extrados. If possible, the z coordinate of the position of the center of the semi-sphere of the pin end is saved. The z coordinate of the position of the center of the semi-sphere is saved before the end of the second loop and before the first loop selected another pin. This value is the biggest z coordinate of the M triangles. Finally, the z coordinates of the positions of the semi-spheres of the

ends of all pins of the punch are obtained and the procedure ends. With the x and y coordinates of the semi-spheres of the ends of the pins are obtained in the previous subsection, the positions of the pins of the punch can then be computed in a similar way for the die.

5. MODELING AND SIMULATION OF THE PRESSING PROCESS WITH RECONFIGURABLE PUNCH AND DIE

The pressing process with configurable punch and die with the geometry set up described in the previous section was modeled with a finite element approach on the ANSYS/LS-DYNA platform. As described previously, the pins were assumed to be rigid bodies. As a result, only the semi-sphere ends of the pins were required to be modeled. In addition, the semi-spheres were assumed as hollow parts with very small thickness. The pins that did not locate in the pressing punch and die zones were not used in the model. The pins were meshed with 4-node shell elements and the numbers of elements and nodes were much less than a mesh with solid elements for solid pins. All pins were identical with a pin diameter of 10 cm. The pressing guides were considered as motionless walls and were also assumed as rigid bodies with very small thickness. Therefore, the pressing guides were also meshed with 4-node shell elements for reducing the numbers of elements and nodes of the model. For all of the shell elements, there were five integration points through the thickness of the element. The part of the model for the blank was the same as for the previous model (i.e., the same material properties, element type and total elements for the pressing process with continuous matched punch and die). The contact type between the blank and the rigid bodies (i.e., the punch, the die and the pressing guides) was automatic node-to-surface with the surfaces of the rigid bodies as contact surfaces and the surfaces of the blank as target surfaces. The static and dynamic friction coefficients on the contact surfaces were 0.6. The reconfigurable die was motionless as was the pressing guides during the process. The complete model is illustrated in Fig. 21.

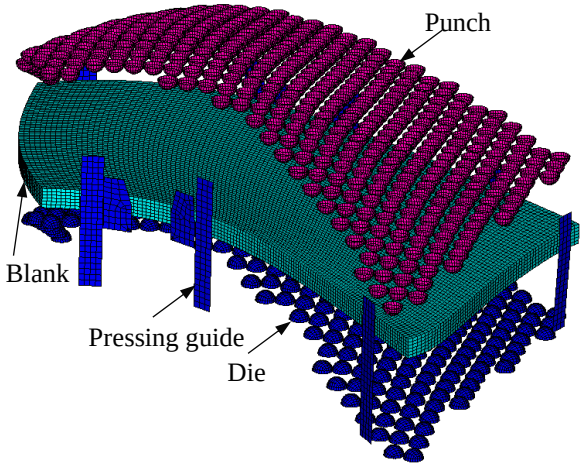

Fig. 21 Model of flexible pressing process with reconfigurable punch and die.

The obtained raw blade is shown in Fig. 22. Figure 23 shows the top surface of the raw blade compared with the one obtained from the simulation of the conventional pressing process.

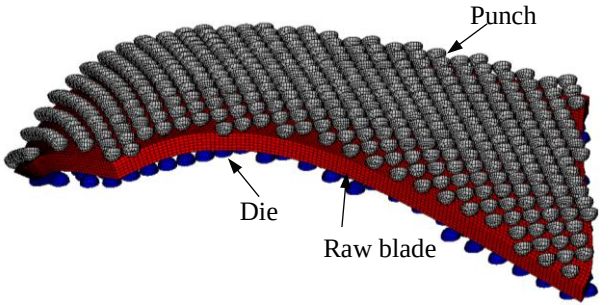

Fig. 22 Model of flexible pressing process with reconfigurable punch and die.

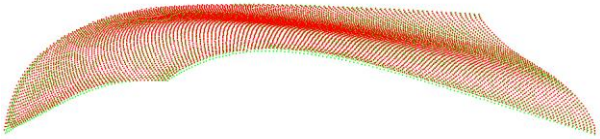

Fig. 23 Comparison between the tops of the raw blades obtained by conventional pressing process (Green points) and the flexible pressing process (Red points).

6. CONCLUSION

In this paper we described the simulation of the pressing process with reconfigurable punch and die. The dies are made of spherical pins assembled altogether in order to represent as close as possible the continuous shapes of conventional pressing matrices.

Comparison between manufacturer's data and both simulations, i.e. conventional punch and die and the reconfigurable ones, show that the reconfigurable option is very satisfactory and could be used for reducing the pressing costs of conventional press forming for small batch. Further investigations about setup frames of reconfigurable dies will be pursued as future works.

ACKNOWLEDGMENTS

The authors express their acknowledgements to the Natural Sciences and Engineering Research Council (NSERC) of Canada, Alstom Hydro Canada Inc. and Hydro Quebec for their financial supports to this research.

REFERENCES

Cai Z.Y., Li M.Z., 2005. Finite element simulation of multi-point sheet forming process based on implicit scheme. Journal of Materials Processing Technology, 161: 449-455.

Chen J.J., Li M.Z., Liu W., Wang C.T., 2005. Sectional multipoint forming technology for large-size sheet metal. International Journal of Advanced Manufacturing Technology, 25: 935-939.

Haas E., Schwarz R.C., Papazian J.M., 2002. Design and test of a reconfigurable forming die. Journal of Manufacturing Processes, 4: 77-85.

Hardt D.E., Olsen B.A., Allison B.T., Pasch K., 1981. Sheet Metal Forming with Discrete Die Surfaces. Manufacturing Engineering Transactions, 140-144.

Heo S.C., Seo Y.H., Park J.W., Ku T.W., Kim J., Kang B.S., 2010. Application of flexible forming process to hull structure forming. Journal of Mechanical Science and Technology, 24: 137-140.

Heo S.C., Seo Y.H., Ku T.W., Kang B.S., 2010. A study on thick plate forming using flexible forming process and its application to a simply curved plate. International Journal of Advanced Manufacturing Technology, 51: 103-115.

Li L., Seo Y.H., Heo S.C., Kang B.S., Kim J., 2010. Numerical simulations on reducing the unloading springback with multi-step multi-point forming technology. International Journal of Advanced Manufacturing Technology, 48: 45-61.

Li M., Liu Y., Su S., Li G., 1999. Multi-point forming: A flexible manufacturing method for a 3-d surface sheet. Journal of Materials Processing Technology, 87: 277-280.

Li M.Z., Cai Z.Y., Liu C.G., 2007. Flexible manufacturing of sheet metal parts based on digitized-die. Robotics and Computer-Integrated Manufacturing, 23: 107-115.

Li M.Z., Cai Z.Y., Sui Z., Yan Q.G., 2002. Multi-point forming technology for sheet metal. Journal of Materials Processing Technology, 129: 333-338.

Papazian J.M., 2002. Tools of change: Mechanical Engineering, 124: 52.

Perzyk M., Kochański A., 2003. Detection of causes of casting defects assisted by artificial neural networks. Proceedings of the Institution of Mechanical Engineers, Part B: Journal of Engineering Manufacture, 217(9): 1279-1284.

Quan G.Z., Ku T.W., Kang B.S., 2011. Improvement of formability for multi-point bending process of AZ31B sheet material using elastic cushion. International Journal of Precision Engineering and Manufacturing, 12: 1023-1030.

Socrate S., Boyce M.C., 2001. A finite element based die design algorithm for sheet-metal forming on reconfigurable tools. Journal of Engineering Materials and Technology, Transactions of the ASME, 123: 489-495.

Walczyk D.F., Hardt D.E., 1998. Design and Analysis of Reconfigurable Discrete Dies for Sheet Metal Forming. Journal of Manufacturing Systems, 17: 436-454.

Walczyk D.F., Hardt D.E., 1999. A comparison of rapid fabrication methods for sheet metal forming dies. Journal of Manufacturing Science and Engineering, Transactions of the ASME, 121: 214-224.

Zhang Q., Dean T.A., Wang Z.R., 2006. Numerical simulation of deformation in multi-point sandwich forming. International Journal of Machine Tools and Manufacture, 46: 699-707.

✧AUTHORS' NOTE

In memory of "Jacques" Zhengkun Feng, our dear friend, who suddenly and very sadly passed away in December 2016.